Quantum wave packet dynamics with trajectories: Reflections on a downhill ramp potential

ARTICLE *in* CHEMICAL PHYSICS LETTERS · JULY 2000

Impact Factor: 1.9 · DOI: 10.1016/S0009-2614(00)00620-5

2 AUTHORS:

Courtney Lopreore

8 PUBLICATIONS **593** CITATIONS

SEE PROFILE

Robert Wyatt

University of Texas at Austin

170 PUBLICATIONS **4,695** CITATIONS

SEE PROFILE

21 July 2000

ELSEVIER

Chemical Physics Letters 325 (2000) 73–78

CHEMICAL PHYSICS LETTERS

www.elsevier.nl/locate/cplett

Quantum wave packet dynamics with trajectories: reflections on a downhill ramp potential

Courtney L. Lopreore, Robert E. Wyatt *

Institute for Theoretical Chemistry and Department of Chemistry and Biochemistry, The University of Texas at Austin, Austin, TX 78712, USA

Received 9 March 2000; in final form 15 May 2000

Abstract

The quantum trajectory method (QTM) for wave packet dynamics involves solving discretized hydrodynamic equations-of-motion in the Lagrangian picture (C. Lopreore, R.E. Wyatt, Phys. Rev. Lett. 82 (1999) 5190). In this Letter, results are presented which illustrate the dynamics of an initial Gaussian wave packet on a downhill ramp potential. Plots are shown for the time evolving probability density, as well as phase space plots and force diagrams. The mechanism, deduced from these plots, surprisingly shows some of the transmitted fluid elements of the wave packet making a U-turn before they head downhill on the ramp potential. © 2000 Published by Elsevier Science B.V.

1. Introduction

Recently much progress has been made in developing and improving numerical approximations for modeling the dynamics of chemical reactions. In a previous paper, Lopreore and Wyatt [1] implemented the quantum trajectory method (QTM), an algorithm based on the hydrodynamic formulation of quantum mechanics introduced by Madelung[2], deBroglie [3,4] and Bohm [5,6] and developed later by several others [7–17]. Among the more recent of these investigations involve works by Sales–Mayor et al. who have successfully applied a Langrangian viewpoint of the hydrodynamic model to molecular photodissociation [13]. Also, Bittner has nicely applied this formulation to dynamics in a harmonic well and tunneling in a double well potential [14]. In the previous study by Lopreore and Wyatt, QTM was applied to one and two-dimensional scattering of quantum trajectories from Eckart barriers. With the success of the results from this investigation and other works [15–17], we are presenting here another case for which this formulation works very well and the results provide insight into an interesting problem in wave packet dynamics.

The problem that we are considering is the evolution of an initial Gaussian wave packet on a one-dimensional downhill ramp potential energy surface. This problem is interesting because it provides deeper insight into the nature of exothermic chemical reactions, as well as sticking reactions, and is also a good model for photodissociation on some excited state potential energy surfaces. Accurately determining

* Corresponding author. Fax: +1-512-471-8696; e-mail: cman041@aurora.hpc.utexas.edu

0009-2614/00/$ - see front matter © 2000 Published by Elsevier Science B.V.
PII: S0009-2614(00)00620-5

transmission/reflection probabilities on the ramp potential has proven to be very challenging for semiclassical theories and has been the subject of a small number of other investigations [18–20]. In a study by Maitra and Heller [20], a semiclassical perturbation approach was introduced for solving the quantum problem of 'reflection above the barrier'. The method incorporated ideas from two widely used approximations in semiclassical theories: the Born perturbative approximation and the semiclassical Wentzel–Kramers–Brillouin wave function. Maitra and Heller's semiclassical perturbative approach successfully determined reflection coefficients from a ramp potential where neither the two aforementioned methods work when considered separately. Similarly, Berry and Mount [18,19] have also presented a discussion on a semiclassical approximation using the Bremmer method for computing quantum reflection coefficients. This method involves a multiple scattering approach, where a smooth potential is approximated by a series of N steps, N being very large. The Bremmer method [21,22] is also accurate in evaluating quantum reflection coefficients on a ramp potential. We are also motivated to study this model because it delves into one of the most interesting quantum phenomena, reflection of probability for energies above a barrier. This is interesting because there are no classical turning points, at least for real valued trajectories. There has been very little research on the mechanism for these processes. We will show that the QTM yields new physical insight on the mechanism for these unique phenomena as well as yielding accurate transmission probabilities. In Section 2, we will review the quantum trajectory method. Section 3 briefly describes the computational procedure, Section 4 defines the model used to illustrate our approach, and Section 5 involves a discussion on the computational results. Finally in Section 6 we conclude with a summary of ideas introduced in this study.

2. The quantum trajectory method

The hydrodynamic equations of motion are derived from the Schrödinger equation analytically [23]. We begin by substituting the polar form of the wave function [2] $\psi = R\mathrm{e}^{\mathrm{i}S/\hbar}$ (R and S are real-valued amplitude and action functions), into the TDSE. Separating into real and imaginary parts we obtain

$$\frac{\partial \rho(\boldsymbol{r},t)}{\partial t} + \boldsymbol{\nabla}\cdot\left(\frac{\rho}{m}\boldsymbol{\nabla} S\right) = 0\,, \tag{1}$$

$$-\frac{\partial S(\boldsymbol{r},t)}{\partial t} = \frac{1}{2m}(\boldsymbol{\nabla} S)^2 + V(\boldsymbol{r},t) + Q(\rho;\boldsymbol{r},t)\,, \tag{2}$$

where the probability density is $\rho(\boldsymbol{r},t) = R(\boldsymbol{r},t)^2$. Since the velocity can be identified as $\boldsymbol{v} = \boldsymbol{\nabla} S/m$ and the flux as $j = \rho\boldsymbol{v}$, Eq. (1) is the continuity equation. Eq. (2) is the quantum Hamilton–Jacobi equation [1] that is identical to the classical Hamilton–Jacobi equation with the exception of the last term. This term, referred to as the quantum potential, is defined by the curvature of the amplitude

$$Q(\rho;\boldsymbol{r},t) = -\frac{\hbar^2}{2m}\frac{1}{R}\nabla^2 R = -\frac{\hbar^2}{2m}\rho^{-1/2}\nabla\rho^{1/2}\,. \tag{3}$$

This equation is responsible for all quantum effects in the QTM. Taking the gradient of Eq. (2) we derive the equation of motion for the flow acceleration

$$m\frac{\mathrm{d}\boldsymbol{v}}{\mathrm{d}t} = -\boldsymbol{\nabla}(V+Q) = \boldsymbol{f}_c + \boldsymbol{f}_q\,, \tag{4}$$

where the Lagrangian ('moving') time derivative is $\mathrm{d}/\mathrm{d}t = \partial/\partial t + \boldsymbol{v}\cdot\boldsymbol{\nabla}$. In Eq. (4) there are two force terms: the 'classical' force arising from the gradient of the potential surface and the quantum force arising form the tilt of the quantum potential.

In order to update the density, an equation in the Lagrangian viewpoint is needed. We can write Eq. (1) as

$$\left(\frac{\partial}{\partial t} + \boldsymbol{v}\cdot\boldsymbol{\nabla}\right)\rho = \frac{\mathrm{d}\rho}{\mathrm{d}t} = -\rho\boldsymbol{\nabla}\cdot\boldsymbol{v}\,. \tag{5}$$

This equation may then be integrated in order to obtain the density propagator

$$\rho(\boldsymbol{r},t+\mathrm{d}t) = \Omega(t+\mathrm{d}t,\mathrm{d}t)\,\rho(\boldsymbol{r},t) = \mathrm{e}^{-(\boldsymbol{\nabla}\cdot\boldsymbol{v})\mathrm{d}t}\rho(\boldsymbol{r},t)\,. \tag{6}$$

Eqs. (4) and (6) are the Lagrangian equations-of-motion in the QTM.

3. Computational procedure

In order to find the solutions of the hydrodynamic equations, we will use a Lagrangian picture in which the solutions are obtained in the same reference frame as the moving fluid. We find it more advantageous to use this viewpoint rather than an Eulerian viewpoint where the equations are solved using fixed in space grids or basis sets. Using this approach, we discretize the probability fluid into N fluid elements ('particles'), each of mass m. As time progresses, the particles will form an unstructured mesh where the distance between them often changes. Hence it is necessary to use a moving grid in order to obtain derivatives, i.e. quantum potential and quantum force. Since we are in a Lagrangian frame, we find it beneficial to use a meshless method, moving weighted least-squares [24,25] (MWLS), in which the fluid particles define the nodes for interpolation. The MWLS algorithm we use to find the derivatives needed in the above equations is similar to one developed for engineering and computational fluid dynamics applications [24,25]. The approximation begins with the assumption that a function $f(\boldsymbol{r})$ is defined on an irregularly spaced set of points. We want an accurate value of f in the vicinity of point $\boldsymbol{r}_i$. Also, there is a basis set (dimension nb) of local polynomials, $p_j(\boldsymbol{r}-\boldsymbol{r}_i)$ so that f can be expanded,

$$f(\boldsymbol{r}) = \sum_{j=1}^{\mathrm{nb}} a_j p_j(\boldsymbol{r}-\boldsymbol{r}_i)\,. \tag{7}$$

The coefficients a_j are approximations to the function and its derivatives at this point $\boldsymbol{r}_i$. In order to find the $\{a_j\}$, we require that the approximation in Eq. (7) passes through np points near point $\boldsymbol{r}_i$. The np points form the *stencil* or *star*. We solve

$$f(\boldsymbol{r}_k) = \sum_{j=1}^{\mathrm{nb}} a_j p_j(\boldsymbol{r}_k-\boldsymbol{r}_i)\,, \quad k=1,2,\ldots,\mathrm{np}\,, \tag{8}$$

in a least squares sense, requiring np > nb (in practice, np = 60, nb = 3). In this one-dimensional problem $p_1 = 1$, $p_2 = x - x_i$, and $p_3 = (x-x_i)^2$. In addition, each equation is assigned a Gaussian weight $w(r_{kl})$ depending on the distance r_{kl} between points k and l. With error minimization for the coefficients $\{a_j\}$, we can find an equation for the solution vector $\boldsymbol{a}$ in terms of the known function vector $\boldsymbol{f}$. We can then use this derivative information for evaluating elements in the hydrodynamic equations-of-motion.

4. Model problem

Now we will apply the QTM to the one-dimensional scattering of an initial Gaussian wave packet (GWP) on a ramp shaped potential energy function. Referring to Landau and Lifshitz [26], the surface is defined as

$$V(x) = \frac{V_o}{1+\mathrm{e}^{\alpha x}}\,, \tag{9}$$

where V_o is the depth and α is the width parameter. In this study, we use Eq. (9) and also consider $V' = -V_o(-x)$ where $V_o = 5000\ \mathrm{cm}^{-1}$ and $\alpha = 1$ a.u. We note that $V(x\to-\infty) = V_o$, $V(0) = V_o/2$, and $V(x\to+\infty) = 0$ in Eq. (9) and $V'(x\to-\infty) = 0$, $V'(0) = -V_o/2$, and $V'(x\to+\infty) = -V_o$. The initial GWP is $(2\beta/\pi)^{1/4}\exp\{-\beta(x-x_o)^2\}$ where $\beta = 8$ a.u. At $t = 0$, the $N = 101$ particles of mass $m = 1867$ are centered at $x_o = 0$ with a spacing of ~ 0.02 a.u., $x_1 = -1$ and $x_{101} = 1$. Fig. 1 shows the initial GWP along with a plot of the model potential energy surface. The ensemble of particles was propagated with time steps of 4 a.u. (0.096 fs).

5. Computational results

The time dependent transmission probability was obtained by integrating ρ on the product side of the

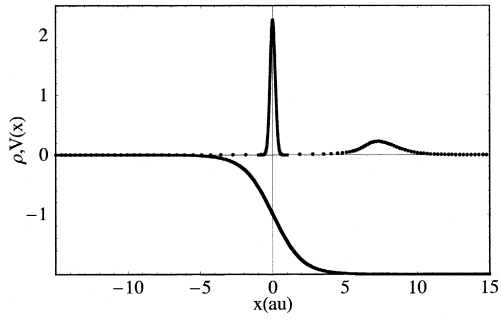

Fig. 1. Probability density plots in atomic units at 0 fs. (solid line) and 48 fs. (dashed line). The downhill ramp potential surface is also shown, but in order to fit on the same plot, the depth has been adjusted to have the value of -2 scaled energy units.

ramp with $x > 0$. In order to compare transmission probabilities to those obtained from the exact quantum result, we implemented an adaptive grid based on the width and location of the wave packet at each time step. This approach is beneficial because less grid points are needed at earlier times when the wave packet is localized. When the packet becomes delocalized, the adaptive grid is useful since more points with smaller spacing are incorporated thus leading to more accurate integral approximations. The density was interpolated at each grid point by averaging over the density of the nearest 10 particles. The results obtained from this procedure at late times agree well with the quantum transmission probability. When $E = 0$, the value of $P(E)$ is 0.989 from the quantum trajectory method; this differs by about 0.7% from the exact value. The same results are obtained when using the second potential energy function, V', described in the previous section.

With the accuracy of the method established, we will now investigate the transmission/reflection mechanism by considering the dynamics of the fluid elements. We first examine the probability density at two different times. Fig. 1 shows the density at 0 and 48 fs. At 48 fs, it is clear that the ensemble of particles has separated into two distinct ensembles traveling in opposite directions since the leading edges of the initial packet are very far from their initial configurations. Also, the spacing of the two particles nearest to the center, $x = 0$, has significantly increased to 1.45 a.u., indicating that the trailing edges of the subensembles are at points of no return.

Now we will investigate the behavior of these trajectories at several time steps. Looking at the phase space plot in Fig. 2a we can see some interesting trends. Fig. 2a is a plot of the central bifurcating trajectories, 30 and 31, as well as a few of their neighbors: Nos. 27–29 and 32–34. Hence, trajectories 1–30 form the reflected ensemble whereas 31–101 form the transmitted ensemble. It is clear from this figure that the bifurcating trajectories evolve under the influence of quite different total forces. The same trajectories are shown in Fig. 2b in a velocity versus time plot. There are several features in Fig. 2b that are worthy of note. First, all of the trajectories acquire a boost in kinetic energy, which leads to the large negative velocity, centered near 5

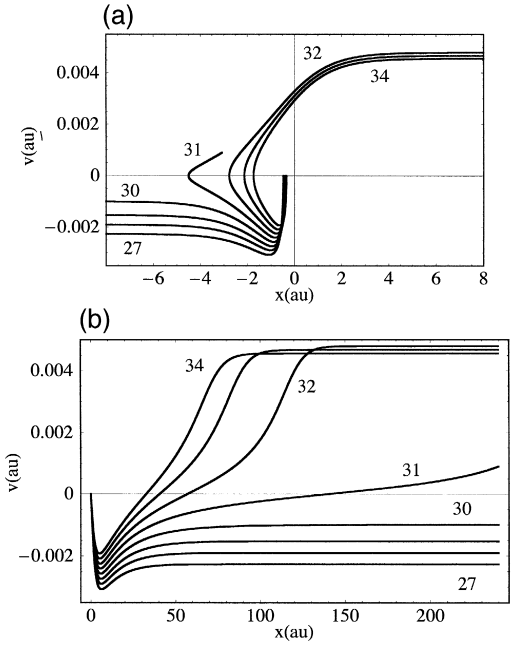

Fig. 2. (a) Phase space diagram for trajectories 27–34; (b) Velocity vs. time for trajectories 27–34 from $t = 0$ to $t = 240$ fs.

fs. Looking at the bifurcating pair during this time, we notice that no. 30 reaches a slightly more negative velocity than no. 31. This negative boost in velocity is enough to allow no. 30 to remain a part of the reflected ensemble. However, for no. 31, the situation is different: this particle reverses direction at $x \sim -4.5$ a.u. and joins the transmitted wave packet. Also, it is interesting to note that each trajectory in the transmitted packet reaches a relatively large positive terminal velocity. This is due to the fact that both the classical and quantum forces go to zero at the flat edges of the potential surface.

Now that we know that the initial boost in kinetic energy plays a significant role in determining which direction the trajectories take, an obvious question is how do the trajectories acquire this boost? This can be better understood if we consider the total forces acting on the particles as well as considering the effects of the quantum potential. Fig. 3a shows the total force acting on trajectories 27–34. Using this plot, we can make several important conclusions about the behavior of the whole trajectory ensemble. The dynamics can be understood as follows: after the

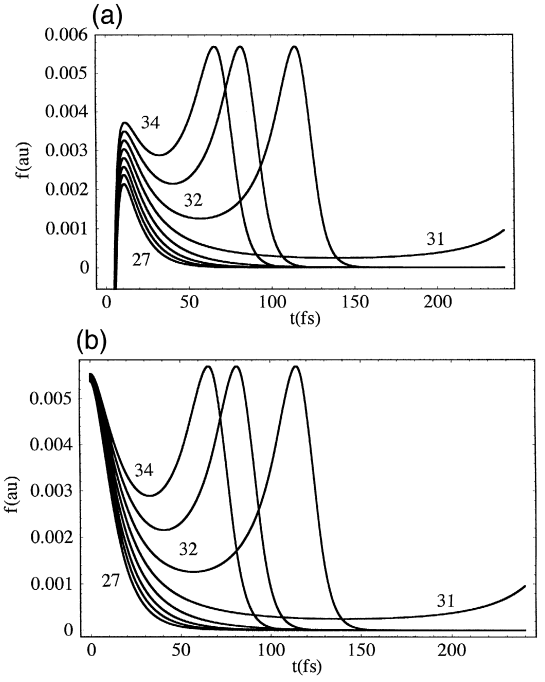

Fig. 3. (a) Total force (quantum + classical) acting on particles 27–34; (b) Classical force acting on particles 27–34.

first time step, the particles on the edges of the packet accelerate in opposite directions due to the forces released from the quantum potential. At this time the quantum potential plays an important role: the edge particles feel a strong force due to the steep slope of the quantum potential. By way of contrast, the centrally located particles feel essentially no quantum force, because the quantum potential is relatively flat in this region. This behavior is not surprising since it is clear from Eq. (3) that the quantum force for the initial GWP is given by

$$f_q = \frac{\hbar^2}{2m}\left[8\beta^2(x - x_o)\right]. \qquad (10)$$

Hence, particles farthest from the center of the packet (x_o) experience a larger magnitude of the quantum force than the ones located closer to the center. Also, the particles on the left leading edge feel a total force which is negative in contrast to those on the right leading edge which feel a positive total force. While Eq. (10) is only accurate for the initial GWP, the same qualitative behavior is still noticed at later times when the packet has expanded. Attenuation of the quantum forces at later times is due to the decreased curvature of the wavefunction which in turn lowers the numerator of the expression for the quantum potential (see Eq. (3)). A short time later, at $t \sim 10$ fs, the edge particles have separated sufficiently beyond their initial locations, the density has decreased, and the quantum force is insignificant. Thus, the trajectories of the particles at later times are dominated by the classical force.

After 10 fs, we mentioned that the classical forces dominate the motion of the trajectories. This is clear since Fig. 3b, a plot of the classical forces acting on particles no. 27–34, shows forces having the same behavior as those in the previous figure. Thus, we can infer that the contribution from the quantum forces occurs only in the first 10 fs. It is interesting to note that if there where no forces due to the potential surface the packet would have separated symmetrically due to the quantum potential. However, the presence of the ramp breaks this symmetry. The transmitted particles acquire additional kinetic energy due to the classical forces acting on them from the downhill nature of the ramp. We can see in Fig. 3b that the classical forces on transmitted trajectories 31–34 decrease, increase, then decrease again. This behavior arises from the fact that initially the transmitted particles 31–34 move uphill due to the large negative value of the quantum force. However, the initial boost in kinetic energy is not sufficient for particles 31–34 to overcome the forces created by the downhill ramp. Once nos. 31–34 lose some of their kinetic energy after going uphill, the classical forces acting on them increase as the particles make their way down the central portion of the ramp. Once they are near the bottom of the surface, the classical forces decrease to zero.

An appealing qualitative picture related to the quantitative features described above is the following: think of the particles as interconnected beads on an elastic string. The beads represent the particles of mass m and the string represents the quantum potential. In this picture, after the first time step, the beads immediately move apart in opposite directions in order to relieve the stress concentrated at the center of the compressed string. As they move apart from the central bead, the beads each acquire a boost in

energy, although some are accelerated to the right and others to the left. This initial boost in kinetic energy ultimately determines whether or not they go down the ramp. In the absence of the quantum potential, the particles are denied an increase in kinetic energy so that none of them will be reflected on the downhill ramp.

6. Summary and conclusion

We have reviewed the quantum trajectory method applied to a one-dimensional ramp potential. The method successfully evaluated the quantum transmission/reflection probability at zero initial kinetic energy. The mechanism extracted from the dynamics of this study suggests an interesting perspective on a quantum phenomenon with no classical turning points. We have demonstrated that the initial wave packet spreads at early times but then later forms two unsymmetrical ensembles representing the transmitted and reflected wave packets. The dynamics of these ensembles indicate that the particles in the QTM experience a boost in kinetic energy at early times due to the quantum potential. This feature is consistent with our earlier findings on barrier transmission [1]. The delicate interplay between the quantum and the classical forces ultimately results in some of the initially reflected particles making a U-turn on the ramp surface, finally becoming members of the transmitted ensemble. This clearly indicates that the QTM can give new insights into how a quantum wave packet evolves on an interesting potential energy surface. It also leads to an intuitive physical picture that cannot be obtained using conventional methods. Since we can exactly solve this realistic but simple quantum system and in the process acquire an intuitive picture, we believe that this method will prove to be useful in investigating more challenging applications.

Acknowledgements

The authors would like to thank Eric Heller for suggesting ideas for this project. We would also like to thank Eric Bittner (University of Houston) for useful discussions and the Texas Advanced Computing Center at the University of Texas at Austin for the use of the Cray SV1, *aurora*. This research was supported by the Robert Welch Foundation and the National Science Foundation.

References

[1] C. Lopreore, R.E. Wyatt, Phy. Rev. Lett. 82 (1999) 5190.
[2] E. Madelung, Z. Phys. 40 (1926) 322.
[3] L. de Broglie, C.R. Acad. Sci. Paris 183 (1926) 447.
[4] L. de Broglie, C.R. Acad. Sci. Paris 184 (1927) 273.
[5] D. Bohm, Phys. Rev. 85 (1952) 166.
[6] D. Bohm, Phys. Rev. 85 (1952) 180.
[7] J.H. Weiner, Y. Partom, Phys. Rev. 187 (1969) 1134.
[8] J.H. Weiner, Y. Partom, Phys. Rev. B 1 (1970) 1533.
[9] J.H. Weiner, A. Askar, J. Chem. Phys. 54 (1971) 1108.
[10] J.H. Weiner, A. Askar, J. Chem. Phys. 54 (1971) 3534.
[11] A. Askar, J.H. Weiner, Am. J. Phys. 39 (1971) 1230.
[12] B.K. Day, A. Askar, H. Rabitz, J. Chem. Phys. 109 (1998) 8770.
[13] F. Sales Mayor, A. Askar, H.A. Rabitz, J. Chem. Phys. 111 (1999) 2423.
[14] E.R. Bittner, J. Chem. Phys. 112 (2000) 9703.
[15] R.E. Wyatt, J. Chem. Phys. 111 (1999) 4406.
[16] R.E. Wyatt, Chem. Phys. Lett. 313 (1999) 189.
[17] R.E. Wyatt, D. Kouri, D. Hoffman, J. Chem. Phys. 112 (2000) 10730.
[18] M.V. Berry, K.E. Mount, Rep. Prog. Phys. 35 (1972) 315, and references therein.
[19] M.V. Berry, J. Phys. A 15 (1982) 3693.
[20] N.T. Maitra, E.J. Heller, Phys. Rev. A 54 (1996) 4763.
[21] H. Bremmer, Physica 15 (1949) 593.
[22] H. Bremmer, Comm. Pure Appl. Math. 4 (1951) 105.
[23] P.R. Holland, The Quantum Theory of Motion, Cambridge Univ. Press, 1993, pp. 68–70.
[24] T. Liszka, Int. J. Numer. Methods Eng. 20 (1984) 1599.
[25] T.J. Liszka, C.A.M. Duarte, W.W. Tworzydlo, Comput. Methods Appl. Mech. Eng. 139 (1996) 263.
[26] L.D. Landau, E.M. Lifshitz, Quantum Mechanics (Nonrelativistic Theory), Oxford, Pergamon, 1965, p. 79.